

Keratin 19, a Cancer Stem Cell Marker in Human Hepatocellular Carcinoma

Takayuki Kawai¹, Kentaro Yasuchika¹, Takamichi Ishii², Hokahiro Katayama¹, Elena Yukie Yoshitoshi¹, Satoshi Ogiso¹, Sadahiko Kita¹, Katsutaro Yasuda¹, Ken Fukumitsu¹, Masaki Mizumoto¹, Etsuro Hatano¹, and Shinji Uemoto¹

Abstract

Purpose: Keratin 19 (K19) is a known marker of poor prognosis and invasion in human hepatocellular carcinoma (HCC). However, the relationship between K19 and cancer stem cells (CSCs) is unclear. Here, we determined whether K19 can be used as a new CSC marker and therapeutic target in HCC.

Experimental Design: HCC cell lines were transfected with a K19 promoter-driven enhanced green fluorescence protein gene. CSC characteristics, epithelial-mesenchymal transition (EMT), and TGFb/Smad signaling were examined in FACS-isolated K19⁺/K19⁻ cells. K19 and TGFb receptor 1 (TGFbR1) expression in 166 consecutive human HCC surgical specimens was examined immunohistochemically.

Results: FACS-isolated single K19⁺ cells showed self-renewal and differentiation into K19⁻ cells, whereas single K19⁻ cells did not produce K19⁺ cells. K19⁺ cells displayed high proliferation

capacity and 5-fluorouracil resistance *in vitro*. Xenotransplantation into immunodeficient mice revealed that K19⁺ cells reproduced, differentiated into K19⁻ cells, and generated large tumors at a high frequency *in vivo*. K19⁺ cells were found to be involved in EMT and the activation of TGFb/Smad signaling, and these properties were suppressed by K19 knockdown or treatment with a TGFbR1 inhibitor. The TGFbR1 inhibitor also showed high therapeutic effect against K19⁺ tumor in the mouse xenograft model. Immunohistochemistry of HCC specimens showed that compared with K19⁻ patients, K19⁺ patients had significantly poorer recurrence-free survival and higher tumor TGFbR1 expression.

Conclusion: K19 is a new CSC marker associated with EMT and TGFb/Smad signaling, and it would thus be a good therapeutic target for TGFbR1 inhibition. *Clin Cancer Res*; 1-11. ©2015 AACR.

Introduction

Recent developments in stem cell biology have revealed the existence of cancer stem cells (CSCs) in various cancers, including leukemia, breast cancer, and colon cancer (1-6). CSCs are a subset of cells with the ability to self-renew, generate a heterogeneous population of cancer cells, and initiate tumor formations (7, 8). These stem-cell-like features of CSCs contribute to rapid tumor growth, tumor resistance to chemotherapy/radiotherapy, and the epithelial-mesenchymal transition (EMT; refs. 9-11). Therefore, CSCs have been attracting increasing attention as a new target for cancer therapies.

Liver cancer, including hepatocellular carcinoma (HCC), is the second leading cause of cancer-related deaths worldwide. Although various therapies have been established and many others are under development, the prognosis of HCC is still poor. In HCC, epithelial cell adhesion molecule (EpcAM), cluster of differentiation (CD) 90, CD133, and sal-like protein 4 have been reported to be useful as CSC surface markers (12-16). However, molecular therapeutic targets for HCC-CSCs remain unestab-

lished. During normal hepatic development, hepatic progenitor cells express both the hepatocyte marker albumin and the cholangiocyte marker keratin 19 (K19; refs. 17, 18). K19 is known to be a marker of poor prognosis in HCC in several studies (19-21). Especially, K19 is reported as a key player in tumor invasion in HCC (22). However, the relationship between K19 and HCC-CSCs is not fully understood. Therefore, based on the similarity between normal tissue stem cells and CSCs, we hypothesized that K19⁺ cells possess CSC characteristics and that K19 is a therapeutic target in HCC.

The aims of this study were to demonstrate that K19⁺ cells have CSC properties in HCC, and to investigate whether K19⁺ cells could be a new therapeutic target. In this study, a transgene vector that expressed green fluorescence protein (EGFP) under the control of the human K19 promoter was transfected into four HCC cell lines to characterize K19⁺ cells as HCC-CSCs. Using FACS-isolated K19⁺/K19⁻ cells, we explored the relationship between K19 and known HCC-CSC markers, the involvement of K19⁺ cells in TGFb/Smad signaling and EMT, and the therapeutic potential of a TGFb receptor 1 (TGFbR1) inhibitor. Moreover, the expression of K19 and TGFbR1 was investigated in human HCC surgical specimens.

Materials and Methods

Patients

This study included 166 consecutive patients with HCC confirmed by pathologic analyses who had undergone a hepatic resection between January 2005 and December 2006 (resection group, *n* = 104) or a liver transplantation between January 2005

¹Department of Surgery, Graduate School of Medicine, Kyoto University, Kyoto, Japan. ²Department of Surgery, Nishikobe Medical Center, Kobe, Japan.

Corresponding Author: Kentaro Yasuchika, Graduate School of Medicine, Kyoto University, 54 Kawara-cho, Shogoin, Sakyo-ku, Kyoto, 606-8507, Japan. Phone: 81-75-751-3242; Fax: 81-75-751-4246; E-mail: kent@kuhp.kyoto-u.ac.jp

doi: 10.1158/1078-0432.CCR-14-1936

©2015 American Association for Cancer Research.

Translational Relevance

Cancer stem cells (CSCs) are strongly associated with various malignant properties of carcinomas, including rapid tumor growth and the epithelial-mesenchymal transition (EMT). Therefore, CSCs have been attracting increasing attention as a new target for cancer therapies. In human hepatocellular carcinoma (HCC), keratin 19 (K19), a marker of hepatic progenitor cell, is known to be a marker of poor prognosis and a key player in tumor invasion. However, the relationship between K19 and HCC-CSCs is not clear. Therefore, we hypothesized that K19⁺ cells possess CSC characteristics and that K19 is a therapeutic target in HCC. Our study indicates that K19⁺ HCC cells possess CSC properties *in vitro* and *in vivo*, which are closely related to TGF β /Smad signaling and EMT, and would be sensitive to a TGF β receptor 1 inhibitor. Further studies on K19⁺ HCC will provide novel therapeutic approaches for HCC treatment.

and December 2008 (transplantation group, $n = 62$) at Kyoto University Hospital. Thirty-four patients fulfilled the Milan criteria for transplantation, and 28 did not. The clinicopathologic characteristics of the subjects are summarized in Supplementary Table S1. Tumor recurrence was investigated until the patient's death or the end of this study (March 31, 2013). No patient was lost to follow-up. The follow-up period from surgery until death or the endpoint of this study was 58 to 2,808 days (mean, 1,581 days) in resection group and 223 to 2,857 days (mean, 1,915 days) in transplantation group.

Written informed consent for the use of resected tissue samples was obtained from all patients in accordance with the Declaration of Helsinki, and this study was approved by the institutional review committee of our hospital.

Construction of the transgene vector

We generated a transgene plasmid vector that expressed EGFP under the control of the human K19 promoter. The promoter activity of the 2952-bp 5'-flanking region of the human K19 gene (from -2952 bp to the first ATG) was previously reported (23). The plasmid vector pHCK-2952, in which the 2952-bp 5'-flanking region of the human K19 gene was inserted into the pGL3-Basic (Promega) vector, was kindly provided by professor Shuichi Kaneko (Kanazawa University, Kanazawa, Japan; ref. 23). We obtained the human K19 promoter region from pHCK-2952 by using *Xho*I and *Hind*III (Takara Bio), and we then ligated it with *Xho*I and *Hind*III-digested plasmid EGFP-1 (pEGFP1; BD Biosciences).

Generation of transgenic HCC cell lines

The human HCC cell lines (Huh7, HLF, PLC/PRF/5, and Hep3B) were obtained from the American Type Culture Collection (ATCC). All cells were authenticated by short tandem repeat profiling before receipt and were propagated for less than 6 months after resuscitation. These cells were cultured at 37°C under 5% CO₂ in RPMI-1640 (Invitrogen) supplemented with 10% FBS (ICN), and penicillin/streptomycin (Meiji Seika).

The transgenic vector was transfected using Lipofectamine LTX (Invitrogen) according to the manufacturer's protocol. Stably

transfected cells were selected in the presence of 200 μ g/mL G418 (Sigma) over 30 days. We confirmed the proper transgene insertion by PCR and immunocytochemistry.

Immunohistochemistry and immunocytochemistry

Immunohistochemistry and immunocytochemistry were performed as previously reported (24, 25). Anti-human K19 mouse antibodies (Dako) diluted at 1:100, anti-human Ki-67 mouse antibodies (BioLegend) diluted at 1:200, anti-TGF β R1 rabbit antibodies (Abcam) diluted at 1:50, and anti-GFP rabbit antibodies (Invitrogen) diluted at 1:200 were used as the primary antibodies. Alexa 488-conjugated or Alexa 594-conjugated goat anti-mouse IgG (Molecular Probes) for K19 staining and Alexa 594-conjugated donkey anti-rabbit IgG (Molecular Probes) for GFP or TGF β R1 staining were used as the secondary antibodies. All secondary antibodies were diluted at 1:500. Two investigators (T. Kawai and K. Yasuchika) independently evaluated the slides.

PCR, quantitative PCR, RT-PCR, and qRT-PCR

The total RNA was extracted with the RNeasy Mini Kit (Qiagen) and RNase-free DNase (Qiagen). The genomic DNA was extracted with the QuickGene-SP Kit (FUJIFILM). The Omniscript Reverse Transcription Kit (Qiagen) was used according to the manufacturer's protocol to reverse transcribe 1 μ g total RNA into cDNA. Primers were generated for the following genes: K19, pEGFP1, CD90, EpCAM, TGF β R1, snail1, slug, E-cadherin, vimentin, multidrug-resistance protein-5 (MRP5), and actin-beta. Their sequences are summarized in Supplementary Table S2. PCR and RT-PCR assays were performed as previously described (26). We performed qPCR and qRT-PCR assays using SYBR-green PCR Master Mix (Applied Biosystems) on the ABI 7500 system (Applied Biosystems). Each target was run in triplicate, and expression levels were normalized to those of actin-beta.

Flow cytometry and single-cell culture analysis

We prepared the cultured cells as described previously (27, 28). Dead cells were eliminated using 7-amino-actinomycin D (Beckman Coulter) staining. To determine the proportion of EpCAM⁺ or CD90⁺ cells, the cells were incubated with phycoerythrin (PE)-conjugated anti-human EpCAM antibody (BioLegend) or PE-conjugated anti-human CD90 antibody (BioLegend) on ice for 30 minutes. PE-conjugated mouse IgG2b (BioLegend) was used as an isotype control for the PE-conjugated EpCAM antibody. PE-conjugated mouse IgG1 (BioLegend) was used as an isotype control of the PE-conjugated CD90 antibody. The cells were analyzed and isolated using a FACSARIA cell sorter (BD Biosciences).

We performed single-cell culture analyses as previously described (27, 28). The individual isolated cells were each sorted into 96-well culture plates using FACSARIA (BD Biosciences). We used a light microscope 10 to 16 hours after cell sorting to confirm that each well contained only one cell. Following cell expansion after isolation of each clone, we subjected the cells to flow cytometry.

Cell proliferation assay, anchorage-independent growth assay, and sphere-forming assay

We inoculated the isolated EGFP⁺ and EGFP⁻ cells differentiated from one EGFP⁺ cell at a density of 1×10^3 cells per

well in 96-well culture plates, which were then allowed to grow for 7 days. The cell numbers were determined using the 3-(4,5-dimethylthiazol-2-yl)-5-(3-carboxymethoxyphenyl)-2-(4-sulfophenyl)-2H-tetrazolium, inner salt (MTS) assay (Cell Titer 96 Aqueous One Solution Reagent; Promega), according to the manufacturer's protocol. After 1 hour of incubation, the absorbance value was measured using a plate reader at 490 nm.

To examine the anchorage-independent growth, 1×10^4 EGFP⁺ and EGFP⁻ cells were suspended in 2.0 mL of 0.3% agar (Wako) supplemented with culture medium. The cell suspension was layered over the bottom layer of 2.0 mL of 0.6% agar. We counted the colonies 14 days after cell sorting.

To investigate the ability to form cell spheres, 1×10^5 EGFP⁺ and EGFP⁻ were seeded in 6-well ultra-low attachment plates (Corning Inc.) in serum-free medium. We observed the spheres 5 days after cell sorting.

Reagents and drug resistance assay

5-Fluorouracil (5-FU) was purchased from Wako and was diluted directly with RPMI-1640 to the desired concentration. The TGF β R1 inhibitor LY2157299 was obtained from Axon Medchem. Compounds were dissolved in 100% dimethyl sulfoxide (DMSO; Sigma) and diluted with RPMI-1640 or saline to the desired concentration with a final DMSO concentration of under 0.5%.

We investigated the resistance of the cells to 5-FU or LY2157299. EGFP⁺ and EGFP⁻ cells were cultured with 5-FU for 96 hours at concentrations of 1×10^{-9} , 1×10^{-7} , 1×10^{-5} , 1×10^{-3} , and 1×10^{-1} mol/L, or with LY2157299 for 72 hours at concentrations of 1×10^{-9} , 1×10^{-8} , 1×10^{-7} , 1×10^{-6} , and 1×10^{-5} mol/L. After the culture, MTS assays were performed to determine the IC₅₀.

Wound-healing assay and migration assay

Wound-healing assays were used to assess capacity for cell motility. We seeded the isolated EGFP⁺ and EGFP⁻ cells differentiated from one EGFP⁺ cell at a density of 1×10^6 cells per well in 35-mm culture dishes. On reaching full confluency, the cell layer was scratched with a 10- μ L plastic tip and then cultured with low serum (2% FBS) culture medium with or without 0.5 μ mol/L LY2157299. Micrographs were taken at 24 or 48 hours after the scratch.

For migration assays, 8- μ m-pore 24-well cell culture plates (Corning Inc.) coated with type I collagen were used. We plated 2.5×10^4 EGFP⁺ and EGFP⁻ cells in the upper chamber with serum-free medium; in the lower chamber, normal culture medium containing 10% FBS was added. After 48 hours of incubation, the cells on the upper surface of the membrane were removed, and the cells on the lower surface were fixed with 4% paraformaldehyde and stained using the Diff-Quick staining Kit (Sysmex).

Western blot analysis

Western blot analysis was performed as previously reported (29). Primary antibodies recognizing phospho-smad2 (pSmad2; Ser465/467, #3108; Cell Signaling), Smad2 (#5339; Cell Signaling), and glyceraldehyde-3-phosphate dehydrogenase (GAPDH; sc-25778; Santa Cruz Biotechnology Inc.) were used at 1:1,000 dilution.

K19 knockdown with RNA interference

We transfected K19-siRNA (#4427037-s7998 or #4427037-s7999; Invitrogen) or control-siRNA (#4390843; Invitrogen)

into HCC cells using Lipofectamine LTX (Invitrogen) according to the manufacturer's protocol. The final concentrations were 10 nmol/L. K19 expression was significantly downregulated by both K19 siRNAs (Supplementary Fig. S1D). According to the same result acquired with both siRNAs, K19-siRNA (#4427037-s7999) was shown as representative data. For Western blot analysis, HCC cells were harvested 48 hours after transfection.

Xenotransplantation

Male 6- to 10-week-old nonobese diabetic/severe combined immunodeficiency (NOD/SCID) mice (Charles River Laboratories, Inc.) were used as recipients for xenotransplantation. The isolated 1×10^4 EGFP⁺ or EGFP⁻ cells derived from a single EGFP⁺ cell were suspended in 200 μ L of a mixture of serum-free medium and Matrigel (BD Biosciences; 1:1 volume). The mixture was injected subcutaneously through a 26-gauge needle into the right and left dorsal areas of anesthetized NOD/SCID mice. We monitored tumor formation and tumor size twice a week, and dissected out the tumors 11 weeks after engraftment.

To investigate the differentiation ability *in vivo*, we performed serial transplantation. Tumors generated from single-cell-derived EGFP⁺ or EGFP⁻ cells were harvested, and then digested with collagenase solution for 30 minutes at 37°C. After rinsing the tumors in PBS, we analyzed and sorted the cells using the FACSaria. Before the second transplantation, the harvested cells were cultured in G418-containing medium for at least 7 days to eliminate cells that originated from the host mice. Thereafter, we sorted these cells according to the EGFP fluorescence, and transplanted 1×10^4 EGFP⁺ or EGFP⁻ cells into NOD/SCID mice in the same way as in the first transplantation.

Experiments on a TGF β R1 inhibitor in a mouse xenograft model

To investigate the therapeutic effect of the TGF β R1 inhibitor *in vivo*, we performed experiments using LY2157299 in a mouse xenograft model. Isolated 1×10^6 EGFP⁺ or EGFP⁻ cells were injected subcutaneously into the right and left dorsal areas of anesthetized NOD/SCID mice. Thereafter, 24 days after the xenotransplantation, we treated twice a day with either saline (control group; $n = 5$) or 75 mg/kg LY2157299 (treated group; $n = 5$) for 10 consecutive days. Tumor size was measured every 3 days for 36 days after engraftment; afterwards, the animals were sacrificed.

All animal experimental procedures were performed according to the Animal Protection Guidelines of Kyoto University.

Statistical analysis

The statistical analyses were performed using SPSS version 17.0 (SPSS Inc.) and GraphPad Prism software version 5.0 (GraphPad Software Inc.). Student *t* test, *F* test, Mann-Whitney *U* test, Fisher exact test, or χ^2 test, and repeated-measures analyses of variances were used for assessment. The mean \pm SD of three or more independent experiments is reported.

Recurrence-free survival (RFS) and overall survival (OS) after the operation were calculated using the Kaplan-Meier method and analyzed with the log-rank test. Significant variables from the univariate analysis were entered in the multivariate analysis using a Cox regression model with forward stepwise selection. Statistical significance was defined as $P < 0.05$.

Results

K19⁺ cells in HCC cell lines

K19 expression was evaluated in the Huh7, PLC/PRF/5, and Hep3B HCC cell lines (Supplementary Fig. S1A). The K19-EGFP reporter vector was transfected into the four HCC cell lines. Huh7, PLC/PRF/5, and Hep3B cells expressed EGFP fluorescence (Supplementary Fig. S1B), whereas HLF cells did not, even though they possessed the transgene in their genomic DNA (Supplementary Fig. S1B). We also confirmed, by immunocytochemistry, that the cells expressing K19 corresponded to the cells expressing EGFP and that the ratio of K19⁺EGFP⁺ to K19⁺ cells was over 95% (Supplementary Fig. S1B). FACS analyses showed that 20.6% ± 3.9% of the Huh7 cells, 14.8% ± 2.7% of the PLC/PRF/5 cells, and 26.7% ± 5.9% of the Hep3B cells ($n = 3$) expressed EGFP (Supplementary Fig. S1C). The sorted EGFP⁺ cells expressed both K19 and EGFP, whereas the sorted EGFP⁻ cells did not express either molecule (Supplementary Fig. S1C). In addition, qPCR assays showed that the K19-EGFP reporter vector was almost equally transfected into both EGFP⁺ and EGFP⁻ cells (Supplementary Fig. S1C). These results indicated that the EGFP⁺ cells corresponded to the K19⁺ cells and that cell sorting could divide the Huh7, PLC/PRF/5, and Hep3B cells according to their K19 production. Therefore, we performed further investigations of the K19⁺ cells in Huh7, PLC/PRF/5, and Hep3B cells to determine whether they were CSCs.

Single-cell culture analysis

We performed single-cell culture analyses to examine self-renewal activity and multipotency. Notably, single K19⁺ Huh7 cells generated both K19⁺ and K19⁻ cell fractions, although single K19⁻ Huh7 cells produced only a K19⁻ cell fraction (Fig. 1A). These findings were reproducible in three trials (three EGFP⁺/EGFP⁻ clones). Similar results were obtained with PLC/PRF/5 and Hep3B cells (Supplementary Fig. S2A). These results indicate that K19⁺ cells have self-renewal activity and the ability to differentiate into K19⁻ cells *in vitro*.

Cell proliferation assay, anchorage-independent growth assay, and sphere-forming assay

Compared with the K19⁻ Huh7 cells, K19⁺ Huh7 cells showed higher proliferation activity ($P < 0.01$, $n = 3$; Fig. 1B) and exhibited a higher ability to form colonies in soft agar ($P < 0.05$, $n = 3$; Fig. 1C). In addition, the sphere assays revealed that K19⁺ Huh7 cells formed cell spheres 5 days after cell sorting, whereas the K19⁻ Huh7 cells did not (Fig. 1C). Similar results were obtained with PLC/PRF/5 and Hep3B cells (Supplementary Fig. S2B and S2C). These findings suggest that the K19⁺ cells have stronger tumorigenic and malignant potential than K19⁻ cells *in vitro*.

Drug resistance to 5-FU

Because CSCs are known to show strong resistance to chemotherapy, we examined 5-FU resistance of K19⁺ and K19⁻ cells.

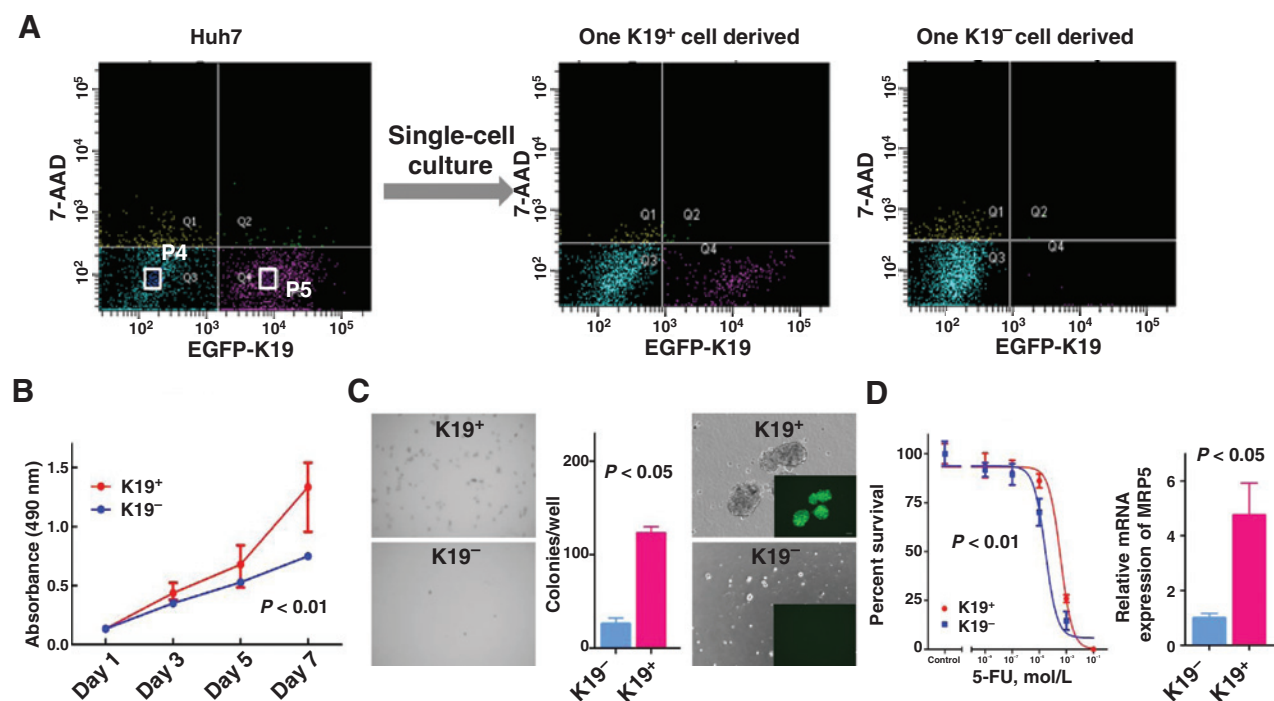
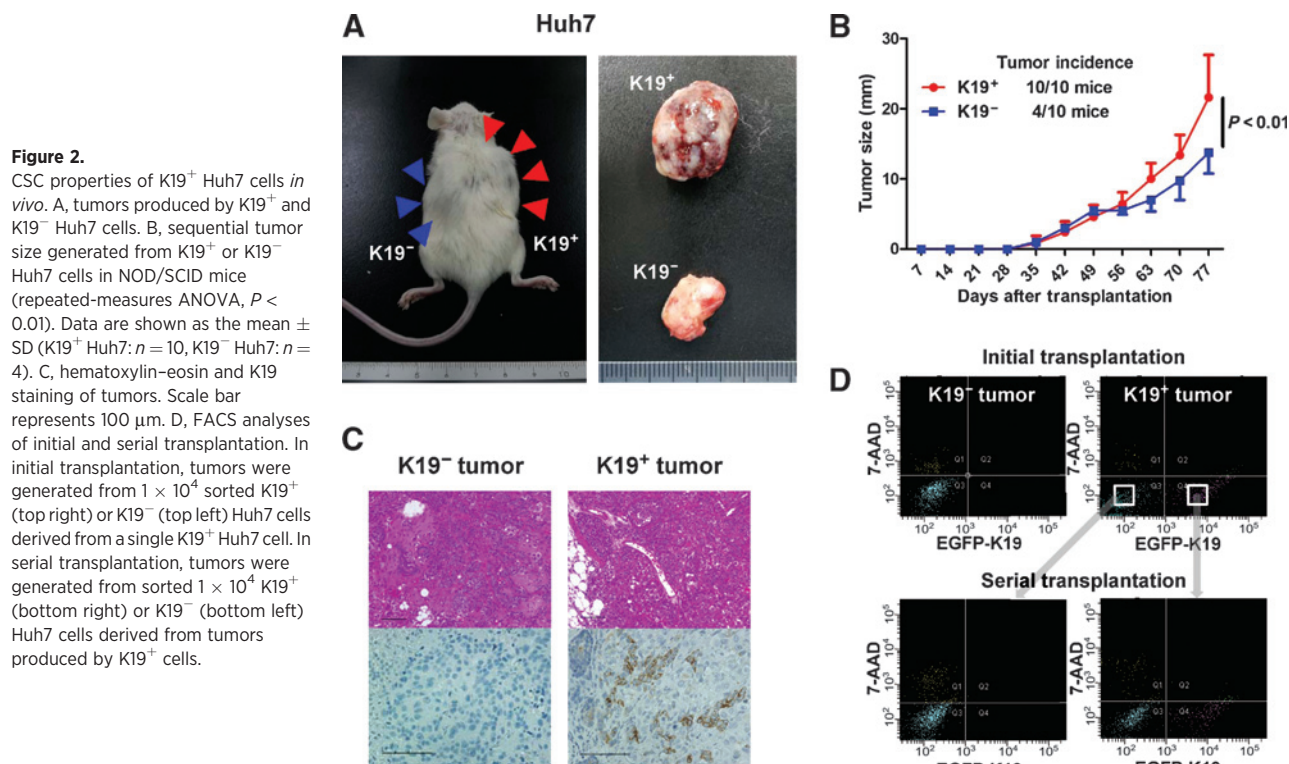


Figure 1.

CSC properties of K19⁺ Huh7 cells *in vitro*. A, single-cell culture analyses of K19⁺ and K19⁻ Huh7 cells. Single K19⁺ cells sorted from P5 quadrangle generated both K19⁺ and K19⁻ cell fractions (middle), whereas single K19⁻ cells sorted from P4 quadrangle produced only K19⁻ cell fractions (right). The vertical axis indicates 7-amino-actinomycin D fluorescence, and the horizontal axis indicates the intensity of enhanced green fluorescence protein-K19. B, cell proliferation assays of K19⁺ and K19⁻ Huh7 cells (repeated-measures ANOVA, $P < 0.01$). C, colony numbers and light microscopic images in the anchorage-independent growth assay (left and middle, Student t test, $P < 0.05$), and phase-contrast images in the sphere-forming assay (right). The original magnification was $\times 20$. D, IC₅₀ of 5-FU in K19⁺ and K19⁻ Huh7 cells (left, F test, $P < 0.01$) and qRT-PCR analyses of K19⁺ and K19⁻ Huh7 cells for multidrug resistance protein-5 (right, Student t test, $P < 0.05$).



The IC₅₀ values for 5-FU were 3.7×10^{-4} mol/L for K19⁺ Huh7, 2.9×10^{-5} mol/L for K19⁻ Huh7, 1.7×10^{-4} mol/L for K19⁺ PLC/PRF/5, 2.8×10^{-5} mol/L for K19⁻ PLC/PRF/5, 2.8×10^{-4} mol/L for K19⁺ Hep3B, and 2.2×10^{-5} mol/L for K19⁻ Hep3B. In all three cell lines, K19⁺ cells were significantly more resistant to 5-FU than K19⁻ cells (Fig. 1D; Supplementary Fig. S2D, $P < 0.01$).

To investigate the mechanism responsible for 5-FU resistance, we analyzed the mRNA expressions of multidrug-resistance protein-5 (MRP5), a key drug transporter for 5-FU (30). qRT-PCR assays of the three cell lines showed that the MRP5 expression of K19⁺ cells was three or more fold higher than that of K19⁻ cells (Fig. 1D; Supplementary Fig. S2D, $P < 0.05$).

Xenotransplantation into immunodeficient mice

To explore CSC properties *in vivo*, we transplanted 1×10^4 K19⁺ or K19⁻ cells derived from one K19⁺ cell into the backs of NOD/SCID mice. K19⁺ Huh7 cells produced larger, hypervascular tumors in 10 of 10 mice, whereas K19⁻ Huh7 cells produced smaller, pale-looking tumors in 4 of 10 mice (Fig. 2A and B). FACS analyses and immunohistological assays revealed that the tumors from K19⁺ cells had both K19⁺ and K19⁻ cell fractions, whereas the tumors from K19⁻ cells had only K19⁻ cell fractions (Fig. 2C and D). In serial transplantation, we transplanted 1.0×10^4 K19⁺ or K19⁻ cells isolated from tumors produced by K19⁺ cells. The tumors derived from K19⁺ cells also contained K19⁺ and K19⁻ cell fractions. In contrast, the tumors derived from K19⁻ cells consisted of only K19⁻ cell fractions (Fig. 2D). Similar results were obtained with PLC/PRF/5 and Hep3B cells (Supplementary Fig. S3A–S3D). These results demonstrate that K19⁺ cells possess the capacity to replicate themselves, to generate heterogeneous lineages of cancer cells, and to initiate tumors *in vivo*.

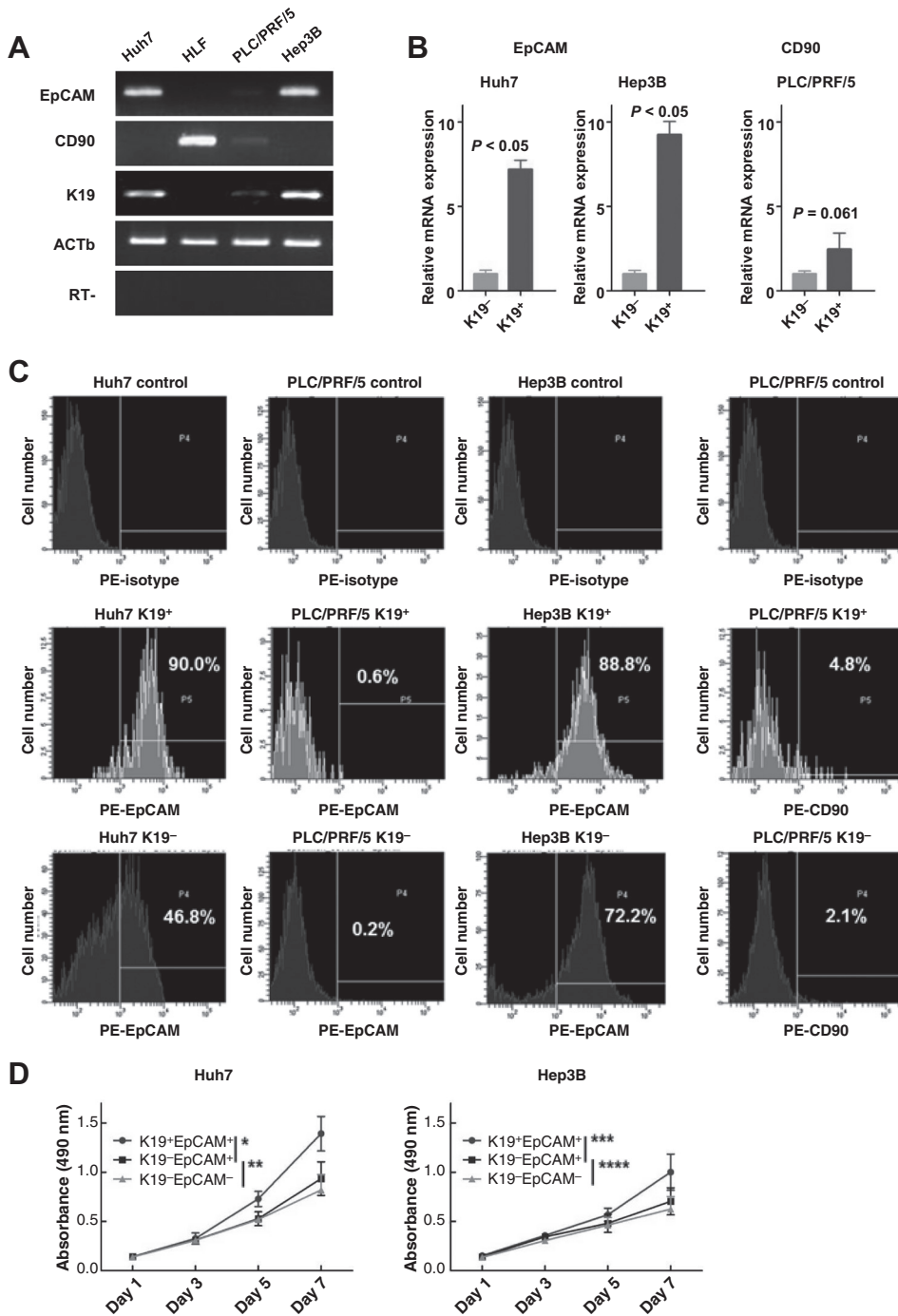
Relationship between K19 and reported HCC-CSCs markers

In the three cell lines that expressed K19, EpCAM expression was observed in Huh7 and Hep3B cells, whereas CD90 expression was observed in HLF and PLC/PRF/5 cells (Fig. 3A). qRT-PCR assays demonstrated significantly higher expression of EpCAM in K19⁺ Huh7 and Hep3B cells than in K19⁻ cells ($P < 0.05$; Fig. 3B). K19⁺ PLC/PRF/5 cells showed higher CD90 expression than K19⁻ cells, although the difference was not statistically significant ($P = 0.061$; Fig. 3B). In FACS analyses, the proportion of EpCAM⁺ cells in K19⁺ Huh7/Hep3B cells tended to be larger than that in K19⁻ cells (Fig. 3C). Only a few CD90⁺ cells were seen in K19⁺ PLC/PRF/5 cells or in K19⁻ PLC/PRF/5 cells (Fig. 3C).

We further explored the growth potential of K19⁺EpCAM⁺, K19⁻EpCAM⁺, and K19⁻EpCAM⁻ cells. Cell proliferation assays indicated that K19⁺EpCAM⁺ Huh7/Hep3B cells had greater proliferation capability than K19⁻EpCAM⁺ cells ($P < 0.01$; Fig. 3D). K19⁻EpCAM⁺ cells showed slightly faster growth than K19⁻EpCAM⁻ cells, although the difference was not statistically significant (Huh7, $P = 0.39$; Hep3B, $P = 0.75$; Fig. 3D). These data suggest that the pattern of K19 expression in K19⁺ HCC cells may be similar to that of EpCAM, and that K19 may play a stronger role than EpCAM in the proliferative capacity of HCC-CSCs.

Involvement of K19 expression in EMT and TGF β /Smad signaling

To investigate the involvement of K19 in EMT and TGF β /Smad signaling, we evaluated the expression pattern of EMT-related markers in HCC cell lines (Fig. 4A). qRT-PCR assays revealed that K19⁺ Huh7 cells showed an EMT gene expression profile: down-regulation of E-cadherin and up-regulation of TGF β R1, snail1, slug, and vimentin ($P < 0.05$; Fig. 4A). Wound-healing and migration assays revealed that K19⁺ cells possessed significantly

**Figure 3.**

Relationship between K19 and reported HCC-CSC markers. A, PCR analysis of HCC cell lines for reported HCC-CSC markers. B, qRT-PCR analysis of K19⁺ and K19⁻ cells for EpCAM (Student *t* test, Huh7, $P < 0.05$; Hep3B, $P < 0.05$) and CD90 (Student *t* test, $P = 0.061$). Data are shown as the mean \pm SD. C, FACS analyses of K19⁺ and K19⁻ cells. The vertical axis indicates the cell number, and horizontal axis indicates the intensity of PE-EpCAM or PE-CD90. D, cell proliferation assays of K19⁺EpCAM⁺, K19⁻EpCAM⁺, and K19⁻EpCAM⁻ cells (repeated-measures ANOVA, *, $P < 0.01$; **, $P = 0.39$; ***, $P < 0.01$; ****, $P = 0.75$).

greater motility than K19⁻ cells (Fig. 4A). This high motility of K19⁺ cells was suppressed by K19 knockdown via RNA interference (Supplementary Fig. S1D). These data indicate that K19⁺ HCC cells have a strong association with EMT.

With the primary focus on strong TGF β R1 expression of K19⁺ cells, we explored TGF β /Smad signaling in K19⁺ cells. Western blot analysis of pSmad2/Smad2 showed that K19⁺ Huh7 cells expressed pSmad2 more strongly than did K19⁻ cells (Fig. 4B). Furthermore, K19 knockdown in Huh7 K19⁺/K19⁻ cells resulted in significant suppression of pSmad2 expression and proliferation

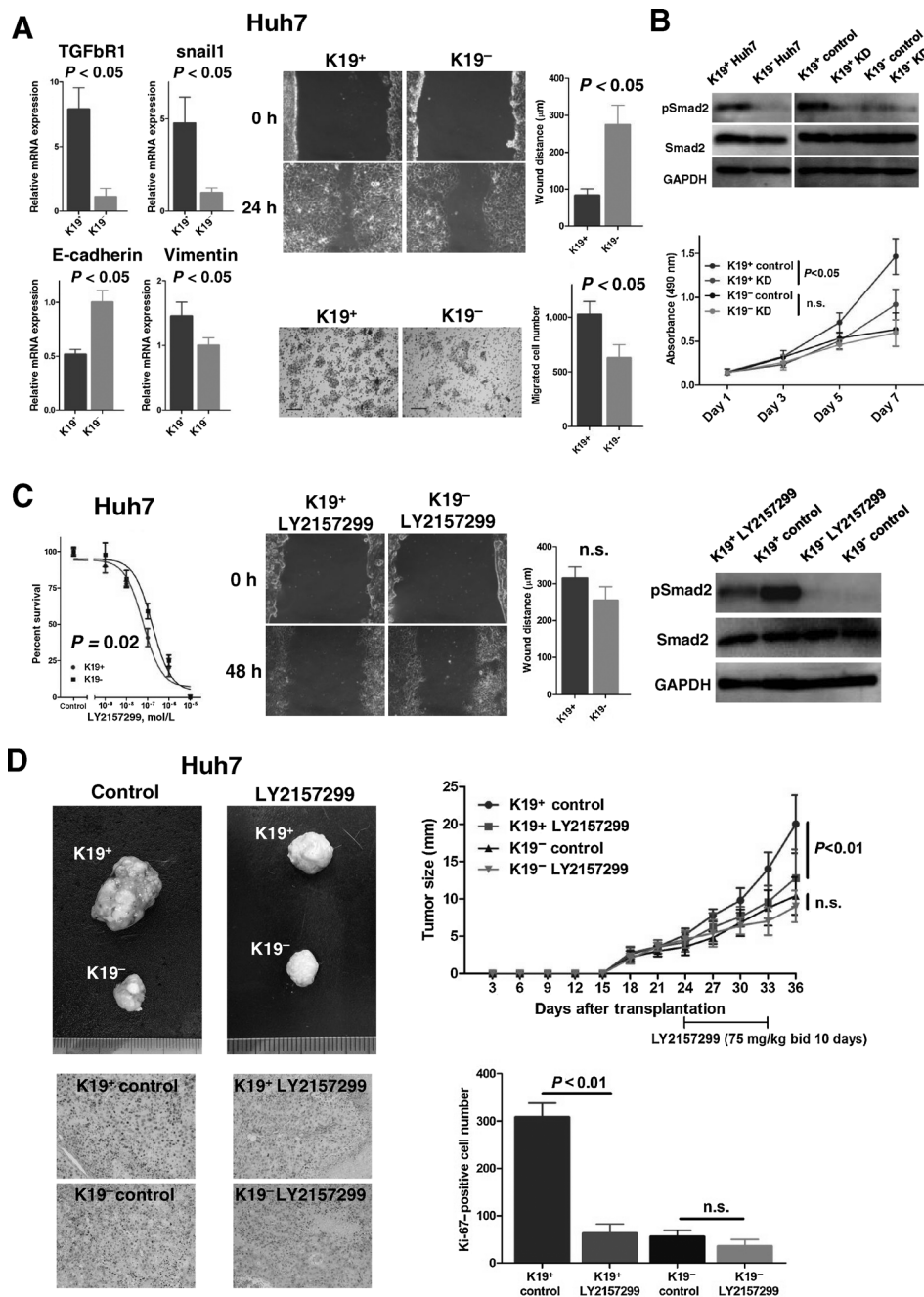
ability in K19⁺ Huh7 cells, whereas these effects were not observed in K19⁻ cells (Fig. 4B). These results indicate that TGF β /Smad signaling is activated in K19⁺ cells and might confer the high proliferation ability to K19⁺ cells.

The effectiveness of the TGF β R1 inhibitor LY2157299 as a new target therapy against K19⁺ cells

We next focused on activation of TGF β /Smad signaling in K19⁺ cells; for this purpose, we examined the effectiveness of LY2157299 to K19⁺ cells *in vitro* and *in vivo*. The IC₅₀ values for

Figure 4.

Involvement of K19 expression in the EMT and TGF β /Smad signaling, and the therapeutic effect of LY2157299 against K19⁺ cells. A, qRT-PCR analysis of K19⁺ and K19⁻ Huh7 cells for EMT-related genes (top, Student *t* test, $P < 0.05$). Data are shown as the mean \pm SD. Phase-contrast images obtained at 0 or 24 hours after the scratch and of the remained wounds at 24 hours after the scratch in wound-healing assays of K19⁺ and K19⁻ cells without LY2157299 treatment (right top, Student *t* test, $P < 0.05$). Original magnification was $\times 20$. Right bottom, migration assays and migrated cell numbers of K19⁺ and K19⁻ cells (Student *t* test, $P < 0.05$). Scale bar represents 100 μ m. B, Western blot analysis for phospho-Smad2 (pSmad2) and Smad2 (top; KD, knockdown by K19-siRNA; control, negative control by control-siRNA). Bottom, cell proliferation assays of K19⁺ and K19⁻ Huh7 cells with K19-siRNA or control-siRNA (repeated-measures ANOVA, K19⁺, $P < 0.05$; K19⁻, n.s.; not significant). C, IC₅₀ values of K19⁺ and K19⁻ cells for LY2157299 (left, *F* test, $P = 0.02$). Middle, phase-contrast images obtained at 0 or 48 hours after the scratch and the remained wounds at 48 hours after the scratch in wound-healing assays with 0.5 μ mol/L LY2157299 treatment (Student *t* test; n.s., not significant). Original magnification was $\times 20$. Right, Western blot analysis of K19⁺ and K19⁻ cells with 24-hour LY2157299 or control treatment for pSmad2 and Smad2. D, tumors produced by K19⁺ and K19⁻ Huh7 cells and sequential tumor size with LY2157299 or control treatment in NOD/SCID mice (repeated-measures ANOVA, K19⁺, $P < 0.01$; K19⁻, n.s., not significant). Data are shown as the mean \pm SD ($n = 5$). Ki-67 staining of tumors and Ki-67-positive cell numbers (bottom, Student *t* test, K19⁺, $P < 0.01$; K19⁻, n.s., not significant).

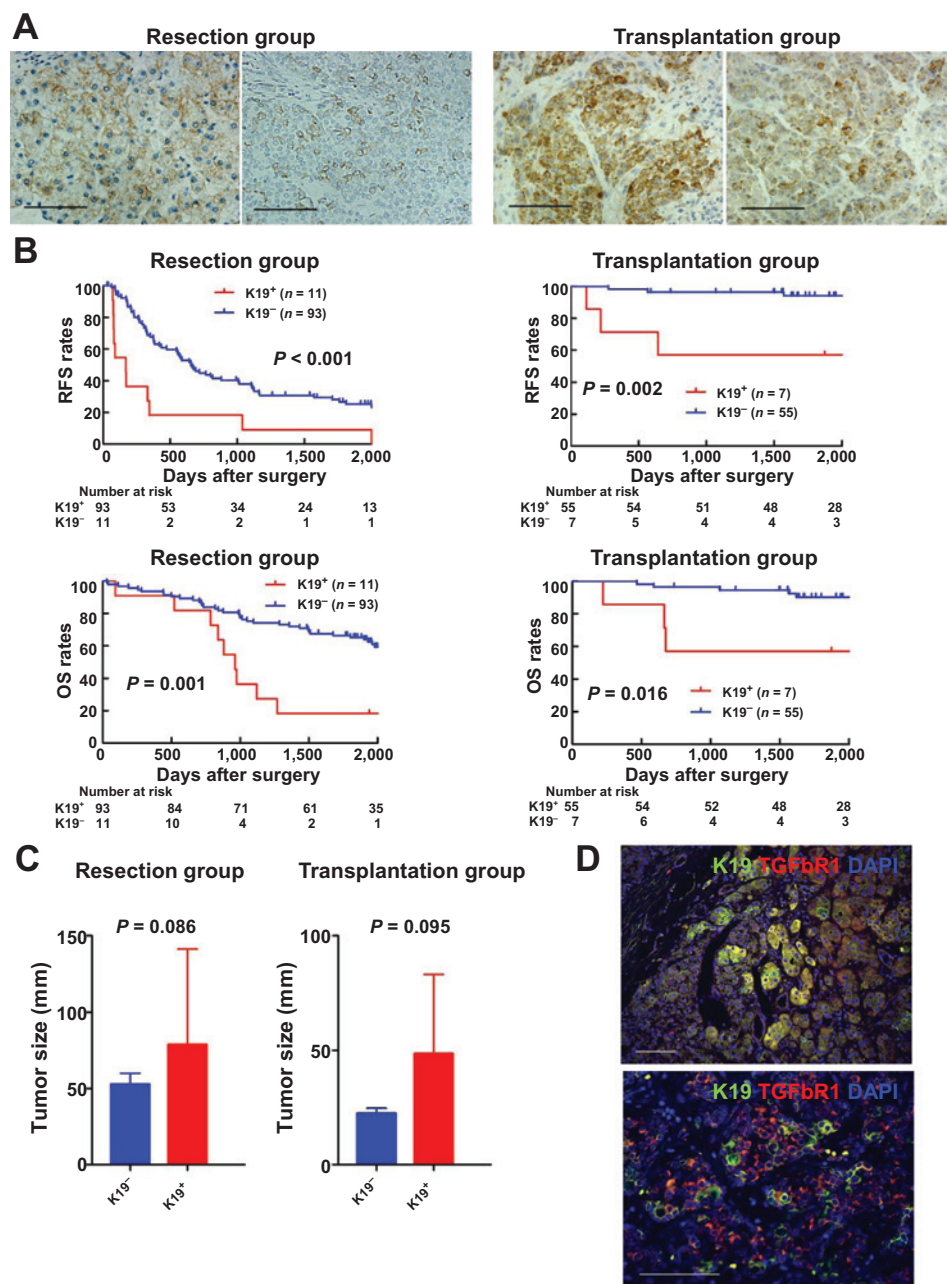


the TGF β R1 inhibitor were 6.2×10^{-8} mol/L for K19⁺ Huh7 and 1.7×10^{-7} mol/L for K19⁻ Huh7 cells. K19⁺ Huh7 cells showed significantly higher sensitivity to LY2157299 than did K19⁻ cells ($P = 0.02$; Fig. 4C). In addition, LY2157299 abolished the motility advantage of K19⁺ cells and suppressed pSmad2 expression in K19⁺ cells (Fig. 4C). Notably, in these experiments, K19⁺ tumors treated with LY2157299 were significantly smaller than K19⁺ tumors treated with saline, whereas LY2157299 showed no significant effectiveness against K19⁻ tumors (K19⁺, $P < 0.01$; K19⁻, n.s., not significant; Fig. 4D). Immunohistochemistry analyses showed that Ki-67-positive cells in LY2157299-treated K19⁺ tumors were significantly

fewer than those in saline-treated K19⁺ tumors. Collectively, these data indicate that LY2157299 would be useful for the treatment of K19⁺ HCC *in vitro* and *in vivo*.

K19 expression in human HCC surgical specimens

To examine K19 expression in human HCC clinical samples, 166 surgically resected HCC tumors were subjected to immunohistochemistry. K19 expression in HCC nodules was observed in 11 of 104 (11%) patients in the resection group and in 7 of 62 (11%) patients in the transplantation group (Fig. 5A). K19 expression was detected in a large proportion or small proportion of HCC tissues (Fig. 5A). In the resection group, the median RFS

**Figure 5.**

Immunohistochemistry analyses of human HCC surgical specimens. A, K19 staining in samples from 2 patients in the resection group (left) and 2 patients in the transplantation group (right). Scale bar represents 100 μm . B, RFS and OS days in the resection group and in the transplantation group according to K19 expression in the HCC tissue. C, tumor size of K19⁺ and K19⁻ patients (Mann-Whitney *U* test, resection group: $P = 0.086$, transplantation group: $P = 0.095$). D, K19 and TGF β R1 staining in samples from 2 HCC patients. Many K19⁺TGF β R1⁺ cells were observed in the invasive front. Scale bar represents 100 μm .

and OS were, respectively, 417 and 1,099 days for K19⁺ patients, and 1,038 and 1,857 days for K19⁻ patients (Fig. 5B). In the transplantation group, the median RFS and OS were, respectively, 1,616 and 1,700 days for K19⁺ patients, and 2,740 and 2,657 days for K19⁻ patients (Fig. 5B). In both groups, K19⁺ patients had significantly lower RFS (resection group, $P < 0.001$; transplantation group, $P = 0.001$) and OS (resection group, $P = 0.002$; transplantation group, $P = 0.016$).

In the resection group, the log-rank test revealed that K19 expression, preoperative low albumin concentration, portal vein invasion, and liver cirrhosis were associated with worsened RFS (Supplementary Table S3). Multivariate analysis demonstrated that K19 expression and portal vein invasion were independent

predictors of postoperative recurrence (Table 1). K19 expression, low albumin concentration, portal vein invasion, and liver cirrhosis were associated with OS by the log-rank test (Supplementary Table S3). Multivariate analysis showed that low albumin concentration, portal vein invasion, and liver cirrhosis were independent predictors of OS, whereas K19 expression was not (Table 1). In the transplantation group, K19 expression, tumor differentiation, and portal invasion significantly decreased both RFS and OS (Supplementary Table S4). Multivariate analysis revealed that K19 expression predicted postoperative recurrence (Table 1). Regarding OS, K19 expression and portal vein invasion were independent predictors of postoperative survival in multivariate analysis (Table 1). In addition, K19 expression tended to

Table 1. Multivariate analysis of factors predicting postoperative prognosis

Variable	HR (95% CI)	P
Postoperative recurrence in the resection group		
K19 expression	2.58 (1.16-5.76)	0.021
Portal invasion	2.01 (1.24-3.25)	0.004
Liver cirrhosis	1.47 (0.90-2.39)	0.121
Albumin (< 3.5 g/dl)	1.39 (0.72-2.66)	0.325
Postoperative survival in the resection group		
Portal invasion	2.15 (1.21-3.83)	0.009
Liver cirrhosis	1.96 (1.09-3.55)	0.026
Albumin (< 3.5 g/dl)	2.00 (1.01-3.94)	0.046
K19 expression	2.04 (0.90-4.63)	0.088
Postoperative recurrence in the transplantation group		
K19 expression	18.4 (1.97-171.3)	0.01
Poorly differentiated	0.75 (0.10-5.58)	0.78
Portal invasion	NA	0.909
Postoperative survival in the transplantation group		
Portal invasion	7.60 (1.63-35.6)	0.01
K19 expression	5.72 (1.21-27.1)	0.028
Poorly differentiated	1.29 (0.28-5.96)	0.75

Abbreviations: CI, confidence interval; K19, cytokeratin 19; NA, not available.

relate to tumor size in the resection (Fig. 5C; $P = 0.086$) and transplantation groups (Fig. 5C; $P = 0.095$).

Correlation between K19 and TGFbR1 expression in human HCC surgical specimens

To investigate the therapeutic potential of a TGFbR1 inhibitor for K19⁺ HCC, we performed double immunofluorescence staining for K19 and TGFbR1 in HCC surgical specimens. TGFbR1 expression in HCC nodules was observed in 9 of 11 (82%) K19⁺ and 18 of 93 (19%) K19⁻ patients in the resection group, and in 5 of 7 (71%) K19⁺ and 15 of 55 (27%) K19⁻ patients in the transplantation group. In K19⁺TGFbR1⁺ patients, TGFbR1 expression was detected in K19⁺ and K19⁻ HCC cells (Fig. 5D). Many K19⁺TGFbR1⁺ cells were seen in the invasive front of HCC (Fig. 5D, top). In both groups, K19 expression was significantly correlated with TGFbR1 expression (resection group, $P < 0.01$; transplantation group, $P = 0.019$).

Discussion

HCC has one of the poorest prognoses among carcinomas, despite advances in treatment such as surgical resection, liver transplantation, radiofrequency ablation (RFA), and regional/systemic chemotherapy. Identification of CSCs and CSC-related therapeutic targets is necessary for improving HCC treatment outcome. Our results showed that K19 can serve as a marker of HCC-CSCs with stem cell characteristics and tumor-initiating capability. Single-cell culture analyses showed that K19⁺ cells had self-renewal ability and differentiation potency, whereas K19⁻ cells could only replicate. Cell proliferation and anchorage-independent growth assays revealed the higher malignant potency of K19⁺ cells. K19⁺ cells were more resistant to 5-FU based on their higher MRP5 expression. In addition, xenotransplantation experiments showed that K19⁺ cells could self-renew, differentiate into K19⁻ cells, and generate larger tumors with a higher incidence *in vivo*. These findings strongly suggest that K19⁺ cells in HCC possess CSC characteristics.

Immunohistochemical analyses of 166 patients revealed that K19 expression was an independent predictor of postoperative recurrence in both resection and transplantation patients, and it was also an independent predictor for OS in the transplantation group. However, in the resection group, K19 expression tended to relate to poor postoperative survival, although the difference was not statistically significant ($P = 0.088$). This result may be attributed to the fact that patients in the resection group have more HCC treatment choices than those in the transplantation group after HCC recurrence, e.g., RFA, transarterial chemoembolization, and systemic chemotherapy. In addition, K19 expression tended to relate to tumor size in both groups, portal invasion in the resection group ($P = 0.09$), and tumor differentiation in the transplantation group ($P = 0.012$). These results indicate that K19⁺ HCC cells with CSC properties could be deeply involved in postoperative early tumor recurrence.

EpCAM and CD90 have been used to identify HCC-CSCs. Our results revealed that K19⁺ cells displayed significantly higher EpCAM gene expression in quantitative RT-PCR analyses and that the K19⁺ cell fraction tended to contain more EpCAM⁺ cells in FACS analyses. Similar to recent studies reporting that EpCAM was associated with tumor size (31), our xenotransplantation assays revealed that K19⁺ cells generated larger tumors. Moreover, a proliferation assay of K19⁺EpCAM⁺, K19⁻EpCAM⁺, and K19⁻EpCAM⁻ cells suggested that K19 may be more strongly associated with rapid tumor growth than EpCAM.

We found that TGFb/Smad signaling was activated in K19⁺ cells and suppressed by K19 knockdown. Moreover, K19 knockdown also suppressed the aggressiveness of K19⁺ cells. These results indicate that TGFb/Smad signaling is involved in conferring the high proliferation ability to K19⁺ cells.

K19 has been reported by Govaere and colleagues (22) as a key player in HCC invasion. They reported that K19-positive HCCs highly express invasion or metastasis-related markers (22). Our results also showed a close correlation between K19 and the EMT which is known as a major mediator of tumor migration/invasion. During EMT, cancer cells shed their epithelial characteristics and acquire more migratory mesenchymal cell-like properties. In this study, we confirmed that K19⁺ cells express several genes associated with EMT and have higher motility and migration than K19⁻ cells. TGFb/Smad signaling is known to increase the growth of cancer cells with mesenchymal properties. Our results suggest that K19⁺ cells acquire mesenchymal characteristics through EMT and exhibit high proliferation ability owing to the activation of TGFb/Smad signaling.

Notably, we found that the TGFbR1 inhibitor LY2157299 would be useful as a new therapy against K19⁺ HCC. K19⁺ cells exhibited high LY2157299 sensitivity in IC₅₀ drug resistance assays. Combined with the result that LY2157299 suppressed the activation of TGFb/Smad signaling in K19⁺ cells, LY2157299 should suppress the aggressiveness of K19⁺ cells through the suppression of TGFb/Smad signaling. The high antitumor effect of LY2157299 to K19⁺ cells was also observed in the mouse xenograft model examined in the present study. Furthermore, immunohistochemistry of samples from HCC patients showed that K19 expression is significantly correlated with TGFbR1 expression. These results suggest that HCC patients with K19 expression could be sensitive to LY2157299. A TGFbR1 inhibitor was reported to block HCC migration, vascular invasion, and

growth through regulation of neoangiogenesis regulation (32–34). Currently, LY2157299 is in phase II clinical trials.

In this study, we were able to isolate K19⁺ and K19⁻ HCC cells. A comprehensive analysis of these cells may detect surrogate marker for a K19 that could be easily evaluated by laboratory tests. Such a marker should be useful in HCC treatments because we could then identify K19⁺ patients without immunohistochemistry or RT-PCR analysis of HCC tissues.

In conclusion, our study indicates that K19⁺ HCC cells possess CSC properties, are closely associated with TGF β /Smad signaling and EMT, and would be sensitive to a TGF β R1 inhibitor. We believe that further studies of K19-related mechanisms will provide novel therapeutic approaches in HCC treatment.

Disclosure of Potential Conflicts of Interest

No potential conflicts of interest were disclosed.

Authors' Contributions

Conception and design: T. Kawai, K. Yasuchika, T. Ishii, S. Ogiso

Development of methodology: T. Kawai, K. Yasuchika

References

- Bonnet D, Dick JE. Human acute myeloid leukemia is organized as a hierarchy that originates from a primitive hematopoietic cell. *Nat Med* 1997;3:730–7.
- Singh SK, Clarke ID, Terasaki M, Bonn VE, Hawkins C, Squire J, et al. Identification of a cancer stem cell in human brain tumors. *Cancer Res* 2003;63:5821–8.
- Al-Hajj M, Wicha MS, Benito-Hernandez A, Morrison SJ, Clarke MF. Prospective identification of tumorigenic breast cancer cells. *Proc Natl Acad Sci U S A* 2003;100:3983–8.
- Collins AT, Berry PA, Hyde C, Stower MJ, Maitland NJ. Prospective identification of tumorigenic prostate cancer stem cells. *Cancer Res* 2005;65:10946–51.
- O'Brien CA, Pollett A, Gallinger S, Dick JE. A human colon cancer cell capable of initiating tumour growth in immunodeficient mice. *Nature* 2007;445:106–10.
- Ricci-Vitiani L, Lombardi DG, Pilozzi E, Biffoni M, Todaro M, Peschle C, et al. Identification and expansion of human colon-cancer-initiating cells. *Nature* 2007;445:111–5.
- Clarke MF, Dick JE, Dirks PB, Eaves CJ, Jamieson CH, Jones DL, et al. Cancer stem cells—perspectives on current status and future directions: AACR Workshop on cancer stem cells. *Cancer Res* 2006;66:9339–44.
- Pardal R, Clarke MF, Morrison SJ. Applying the principles of stem-cell biology to cancer. *Nat Rev Cancer* 2003;3:895–902.
- Dean M, Fojo T, Bates S. Tumour stem cells and drug resistance. *Nat Rev Cancer* 2005;5:275–84.
- Phillips TM, McBride WH, Pajonk F. The response of CD24(-/low)/CD44 +breast cancer-initiating cells to radiation. *J Natl Cancer Inst* 2006;98:1777–85.
- Pattabiraman DR, Weinberg RA. Tackling the cancer stem cells - what challenges do they pose? *Nat Rev Drug Discov* 2014;13:497–512.
- Yamashita T, Ji J, Budhu A, Forgues M, Yang W, Wang HY, et al. EpCAM-positive hepatocellular carcinoma cells are tumor-initiating cells with stem/progenitor cell features. *Gastroenterology* 2009;136:1012–24.
- Ma S, Chan KW, Hu L, Lee TK, Wo JY, Ng IO, et al. Identification and characterization of tumorigenic liver cancer stem/progenitor cells. *Gastroenterology* 2007;132:2542–56.
- Ma S, Tang KH, Chan YP, Lee TK, Kwan PS, Castilho A, et al. miR-130b Promotes CD133(+) liver tumor-initiating cell growth and self-renewal via tumor protein 53-induced nuclear protein 1. *Cell Stem Cell* 2010;7:694–707.
- Yang ZF, Ho DW, Ng MN, Lau CK, Yu WC, Ngai P, et al. Significance of CD90 +cancer stem cells in human liver cancer. *Cancer Cell* 2008;13:153–66.
- Oikawa T, Kamiya A, Zeniya M, Chikada H, Hyuck AD, Yamazaki Y, et al. Sal-like protein 4 (SALL4), a stem cell biomarker in liver cancers. *Hepatology* 2013;57:1469–83.
- Oertel M, Menthen A, Chen YQ, Teisner B, Jensen CH, Shafritz DA. Purification of fetal liver stem/progenitor cells containing all the repopulation potential for normal adult rat liver. *Gastroenterology* 2008;134:823–32.
- Chiba T, Kamiya A, Yokosuka O, Iwama A. Cancer stem cells in hepatocellular carcinoma: Recent progress and perspective. *Cancer Lett* 2009;286:145–53.
- Uenishi T, Kubo S, Yamamoto T, Shuto T, Ogawa M, Tanaka H, et al. Cytokeratin 19 expression in hepatocellular carcinoma predicts early postoperative recurrence. *Cancer Sci* 2003;94:851–7.
- Durnez A, Verslype C, Nevens F, Fevery J, Aerts R, Pirenne J, et al. The clinicopathological and prognostic relevance of cytokeratin 7 and 19 expression in hepatocellular carcinoma. A possible progenitor cell origin. *Histopathology* 2006;49:138–51.
- Kim H, Choi GH, Na DC, Ahn EY, Kim GI, Lee JE, et al. Human hepatocellular carcinomas with "Stemness"-related marker expression: keratin 19 expression and a poor prognosis. *Hepatology* 2011;54:1707–17.
- Govaere O, Komuta M, Berkers J, Spee B, Janssen C, de Luca F, et al. Keratin 19: a key role player in the invasion of human hepatocellular carcinomas. *Gut* 2014;63:674–85.
- Kagaya M, Kaneko S, Ohno H, Inamura K, Kobayashi K. Cloning and characterization of the 5'-flanking region of human cytokeratin 19 gene in human cholangiocarcinoma cell line. *J Hepatol* 2001;35:504–11.
- Ishii T, Yasuchika K, Fujii H, Hoppo T, Baba S, Naito M, et al. In vitro differentiation and maturation of mouse embryonic stem cells into hepatocytes. *Exp Cell Res* 2005;309:68–77.
- Ishii T, Yasuchika K, Machimoto T, Kamo N, Komori J, Konishi S, et al. Transplantation of embryonic stem cell-derived endodermal cells into mice with induced lethal liver damage. *Stem Cells* 2007;25:3252–60.
- Ishii T, Fukumitsu K, Yasuchika K, Adachi K, Kawase E, Suemori H, et al. Effects of extracellular matrixes and growth factors on the hepatic differentiation of human embryonic stem cells. *Am J Physiol Gastrointest Liver Physiol* 2008;295:G313–21.
- Ishii T, Yasuchika K, Suemori H, Nakatsuji N, Ikai I, Uemoto S. Alpha-fetoprotein producing cells act as cancer progenitor cells in human cholangiocarcinoma. *Cancer Lett* 2010;294:25–34.
- Sasaki N, Ishii T, Kamimura R, Kajiwara M, Machimoto T, Nakatsuji N, et al. Alpha-fetoprotein-producing pancreatic cancer cells possess cancer stem cell characteristics. *Cancer Lett* 2011;308:152–61.

Acquisition of data (provided animals, acquired and managed patients, provided facilities, etc.): T. Kawai, S. Ogiso, E. Hatano
Analysis and interpretation of data (e.g., statistical analysis, biostatistics, computational analysis): T. Kawai, K. Yasuchika, K. Fukumitsu
Writing, review, and/or revision of the manuscript: T. Kawai, K. Yasuchika, S. Ogiso, E. Hatano, S. Uemoto
Administrative, technical, or material support (i.e., reporting or organizing data, constructing databases): H. Katayama, E.Y. Yoshitoshi, S. Ogiso, S. Kita, K. Yasuda, K. Fukumitsu, M. Mizumoto
Study supervision: K. Yasuchika, T. Ishii, H. Katayama, E.Y. Yoshitoshi, S. Ogiso, S. Kita, K. Yasuda, K. Fukumitsu, M. Mizumoto, S. Uemoto

Acknowledgments

The authors thank Dr. Makiko Kagaya and professor Shuichi Kaneko (Kanazawa University, Kanazawa, Japan) for plasmid vector pHCK-2952.

Grant Support

This work was supported by grants from the Scientific Research Fund of the Japan Science and Technology Agency (research project number: 24791409).

Received August 6, 2014; revised February 11, 2015; accepted March 10, 2015; published OnlineFirst March 27, 2015.

29. Yamanaka K, Hatano E, Narita M, Kitamura K, Yanagida A, Asechi H, et al. Olprinone attenuates excessive shear stress through up-regulation of endothelial nitric oxide synthase in a rat excessive hepatectomy model. *Liver Transpl* 2011;17:60–9.
30. Pratt S, Shepard RL, Kandasamy RA, Johnston PA, Perry W, Dantzig AH. The multidrug resistance protein 5 (ABCC5) confers resistance to 5-fluorouracil and transports its monophosphorylated metabolites. *Mol Cancer Ther* 2005;4:855–63.
31. Yamashita T, Honda M, Nakamoto Y, Baba M, Nio K, Hara Y, et al. Discrete nature of EpCAM+ and CD90+ cancer stem cells in human hepatocellular carcinoma. *Hepatology* 2013;57:1484–97.
32. Fransvea E, Angelotti U, Antonaci S, Giannelli G. Blocking transforming growth factor-beta up-regulates E-cadherin and reduces migration and invasion of hepatocellular carcinoma cells. *Hepatology* 2008;47:1557–66.
33. Mazzocca A, Fransvea E, Lavezzari G, Antonaci S, Giannelli G. Inhibition of transforming growth factor beta receptor I kinase blocks hepatocellular carcinoma growth through neo-angiogenesis regulation. *Hepatology* 2009;50:1140–51.
34. Dituri F, Mazzocca A, Peidrò FJ, Papappicco P, Fabregat I, DeSantis F, et al. Differential inhibition of the TGF- β signaling pathway in HCC cells using the small molecule inhibitor LY2157299 and the D10 monoclonal antibody against TGF- β receptor type II. *PLoS One* 2013;8:e67109.

Clinical Cancer Research

Keratin 19, a Cancer Stem Cell Marker in Human Hepatocellular Carcinoma

Takayuki Kawai, Kentaro Yasuchika, Takamichi Ishii, et al.

Clin Cancer Res Published OnlineFirst March 27, 2015.

Updated version	Access the most recent version of this article at: doi: 10.1158/1078-0432.CCR-14-1936
Supplementary Material	Access the most recent supplemental material at: http://clincancerres.aacrjournals.org/content/suppl/2015/04/01/1078-0432.CCR-14-1936.DC1.html

E-mail alerts	Sign up to receive free email-alerts related to this article or journal.
Reprints and Subscriptions	To order reprints of this article or to subscribe to the journal, contact the AACR Publications Department at pubs@aacr.org .
Permissions	To request permission to re-use all or part of this article, contact the AACR Publications Department at permissions@aacr.org .